CHAPTER 3

RESULTS AND DISSCUSSION

The results and discussion are separated into two parts: Lanthanum and Cerium Phosphate. They are the following.

3.1 Synthesis of Lanthanum Phosphate ($LaPO_4$) by microwave radiation method

3.1.1 Formation of Lanthanum Phosphate complex

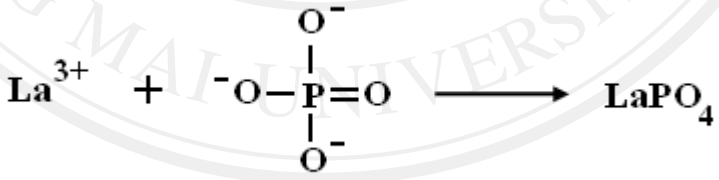

Figure 3.1 Molecular structure of Lanthanum Phosphate.

In this research, the Lanthanum Phosphate ($LaPO_4$) complex was prepared by microwave radiation method. Lanthanum (III) chloride heptahydrate ($LaCl_3 \cdot 7H_2O$) and tri-sodium phosphate ($Na_3PO_4 \cdot 12H_2O$), as starting reagent, were dissolved in 80 ml deionized water. Nitric acid (HNO_3) was used for adjusting pH value of the

precursor solutions to 1-6. Each of solutions was continuously heated by a microwave oven at a time at 180 W for 60 min. The final products were analyzed using XRD, FTIR, SEM, TEM, UV-Vis-NIR and PL spectroscopy.

In this experiment, the pH value of the precursor solutions was study. Because of the previous research showed that the pH value has effected to the phase purity, crystalline structure and morphology of the complex such as yitrium orthovanadate [22], barium titanate [35], tungsten oxide [36] and so on. In this work, the research paid attention on the effect from the pH value of the precursor solutions to the phase purity, structure, morphology, particle size and optical property of $LaPO_4$ as-synthesized [22, 35-37].

3.1.2 X-ray diffraction (XRD)

Phase and crystalline structure of $LaPO_4$ synthesized by microwave radiation method with pH adjusting to be 1-6 by 37 % HNO_3 were investigated by XRD, as shown in Fig. 3.2. These patterns were identified as purified hexagonal $LaPO_4$ phase, comparing to the JCPDS No. 04-0635 (a = b = 7.0420 Å and c = 6.4490 Å). No impurities were detected that show products are very high purities hexagonal $LaPO_4$ phase. When the precursor pH values were lowered from 6 to 1, the XRD peaks became sharper, proving that the product crystal has improved. Therefore, it can be concluded that hexagonal $LaPO_4$ crystalline was influenced by the precursor pH.

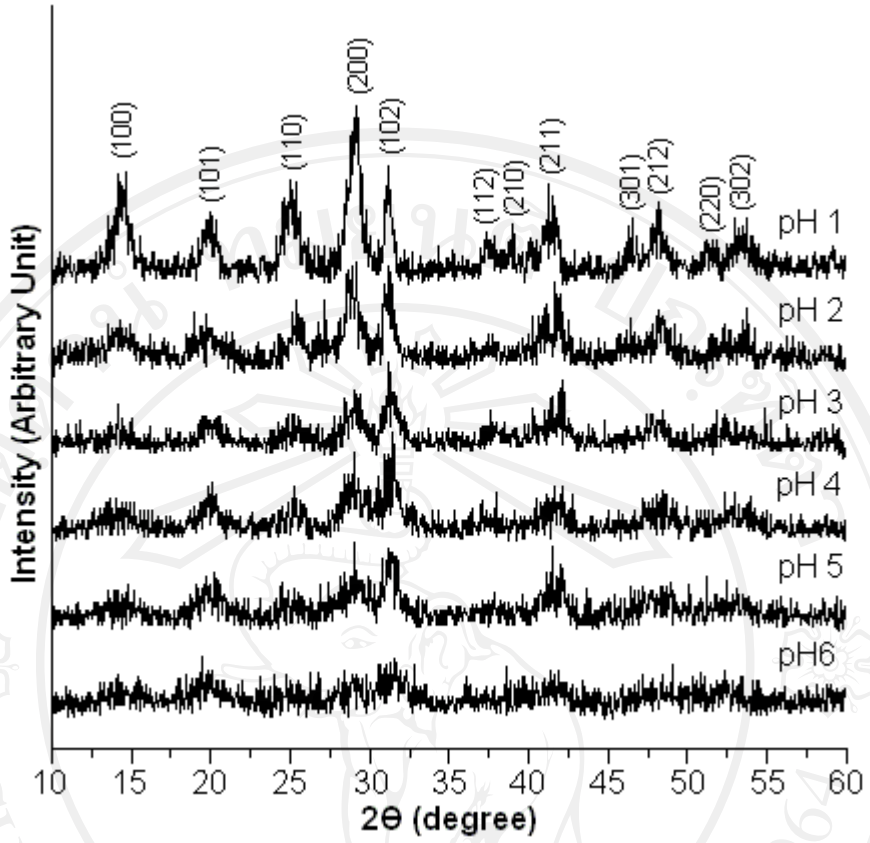

Figure 3.2 XRD patterns of $LaPO_4$ at pH values of 1-6 synthesized by microwave radiation method at 180 W for 60 min.

Lattice parameters of hexagonal $LaPO_4$ nanostructures were calculated from the equation of plane spacing for the hexagonal structure in combination with the Bragg's law for diffraction, as shown below ;

$$\frac{1}{d^2} = \frac{4}{3a^2}\left(h^2 + hk + k^2\right) + \frac{1}{c^2}l^2 \qquad (3.1)$$

$$\lambda = 2d\sin\theta \qquad (3.2)$$

where a and c are the lattice parameters, h, k and l the Miller indices, d the plane spacing, and θ the Bragg's angle. The calculated lattice parameters of the

hexagonal $LaPO_4$ nanomaterials are a = b = 7.0859 Å and c = 6.5016 Å - very close to the JCPDS standard values.

3.1.3 Fourier transforms infrared spectroscopy (FT-IR)

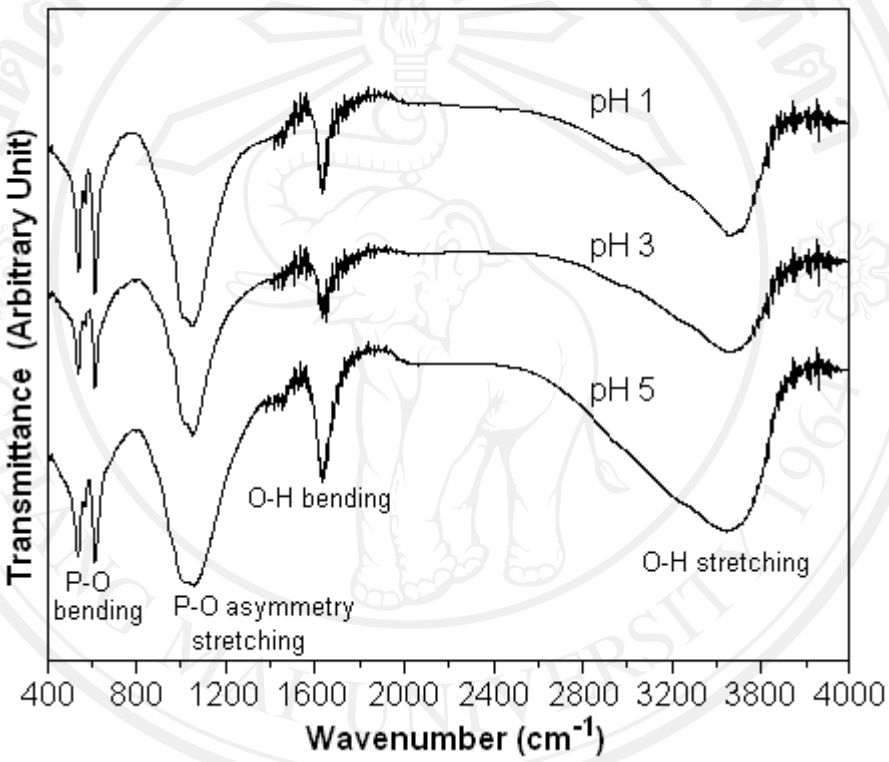

Figure 3.3 FT-IR spectra of $LaPO_4$ synthesized by microwave radiation method at the pH of 1, 3 and 5.

Consider the lanthanide phosphate compounds such as $CePO_4$, $LaPO_4$ and $GdPO_4$. Their different modes were originated from the vibration in the tetrahedral PO_4^{3-} units. The selection rule for the isolated PO_4^{3-} tetrahedrons shows different vibration modes as $A_1(R) + E(R) + 2F_2(IR+R)$. The $\upsilon_1(A_1)$ and $\upsilon_2(E)$ corresponding to the symmetric stretching and bending modes are Raman active. The $\upsilon_3(F_2)$ and $\upsilon_4(F_2)$

are the asymmetric stretching and bending modes, specified as Raman and IR doubly active. The symmetry of PO_4^{3-} ions in the lanthanide phosphate compound decreases from T_d to C_1. Thus, the non-IR modes become IR active [38]. FT-IR spectra of $LaPO_4$ synthesized by the microwave-assisted synthesis at the pH levels of 1, 3 and 5 were recorded in the range 400-4,000 cm^{-1} as shown in Figure 3.3. The broad and sharp peaks at 3440 and 1644 cm^{-1} were, respectively, assigned to be the O-H stretching and bending modes of adsorbed water containing in the product. The other peaks at 1046, 614 and 540 cm^{-1} were seen in the vibrations PO_4^{3-} of $LaPO_4$. The mode at 1046 cm^{-1} was ascribed as the asymmetric stretching vibration of P-O bonds. Those centers at 614 and 540 cm^{-1} were the P-O bending vibrations of the PO_4^{3-} group [37-39]. There were no other functional groups, detected in these products.

3.1.4 Scanning electron microscope (SEM)

The morphologies of $LaPO_4$ nanostructures were characterized by SEM. Due to the SEM analysis (Figure 3.4-3.9), they showed that the morphologies of as-synthesized $LaPO_4$ products have a different shape (nanoparticles and nanorods), depending on the precursor pH of the system. At the pH range of 4-6, they were agglomerates of nanoparticles with their size less than 50 nm. When the precursor pH was lower to 3, the $LaPO_4$ nanoparticles arranged themselves and diffused to form short nanorods. Finally, the short nanorods (~200 nm) and long nanorods (~600 nm) were, respectively, produced at the pH of 2 and 1, under the microwave radiation. These results confirmed that pH is a key factor to control the $LaPO_4$ morphologies, by

changing from nanoparticles to 1-D nanorods, due to the increase in the H^+ concentration of the solutions.

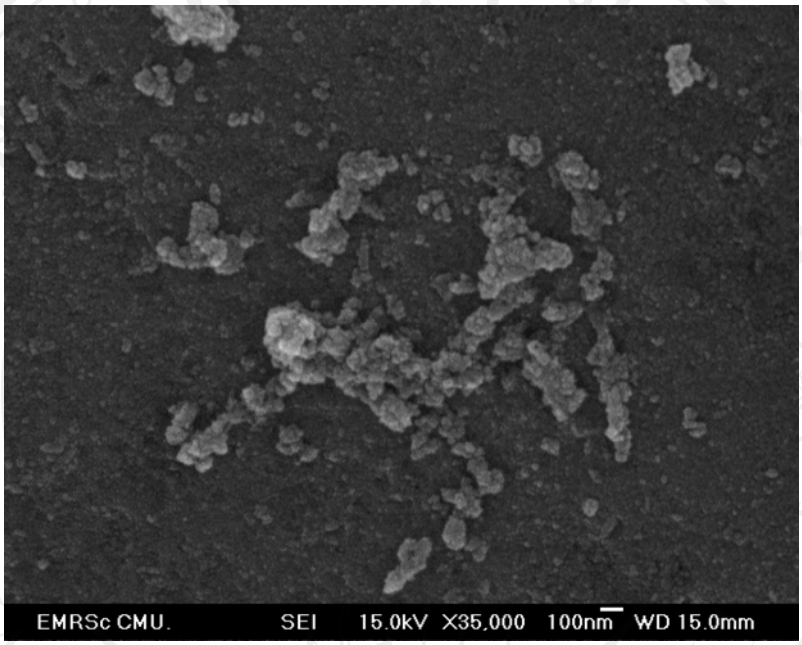

Figure 3.4 SEM image of $LaPO_4$ synthesized in the solution with the pH of 6 by microwave radiation at 180 W for 60 min.

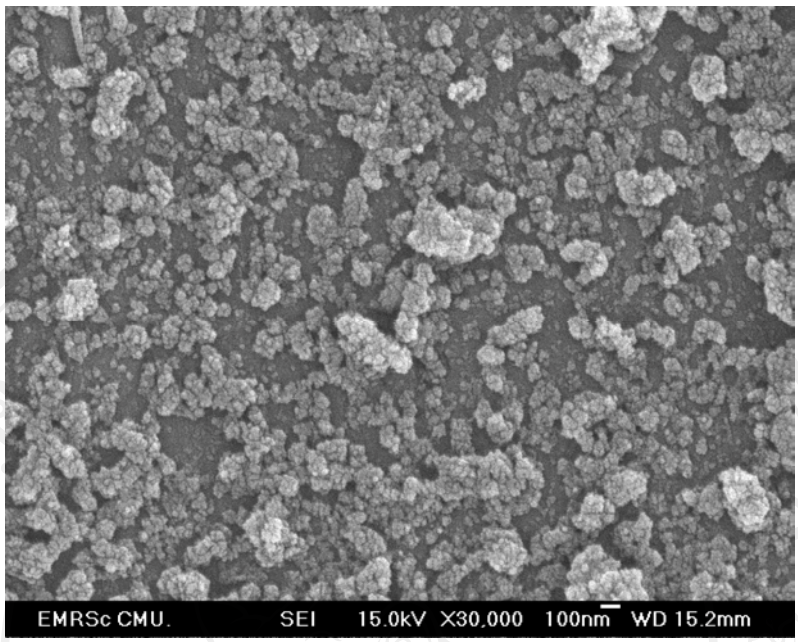

Figure 3.5 SEM image of $LaPO_4$ synthesized in the solution with the pH of 5 by microwave radiation at 180 W for 60 min.

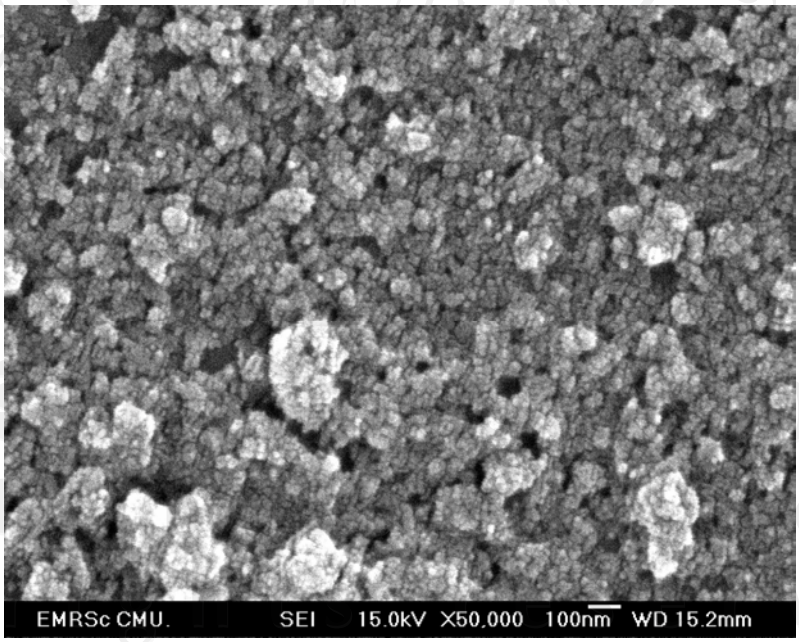

Figure 3.6 SEM image of $LaPO_4$ synthesized in the solution with the pH of 4 by microwave radiation at 180 W for 60 min.

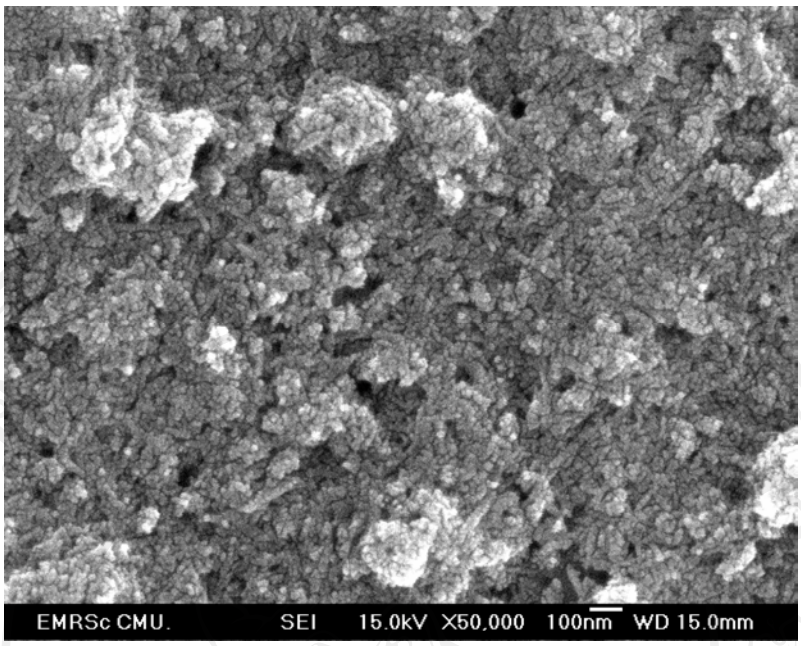

Figure 3.7 SEM image of $LaPO_4$ synthesized in the solution with the pH of 3 by microwave radiation at 180 W for 60 min.

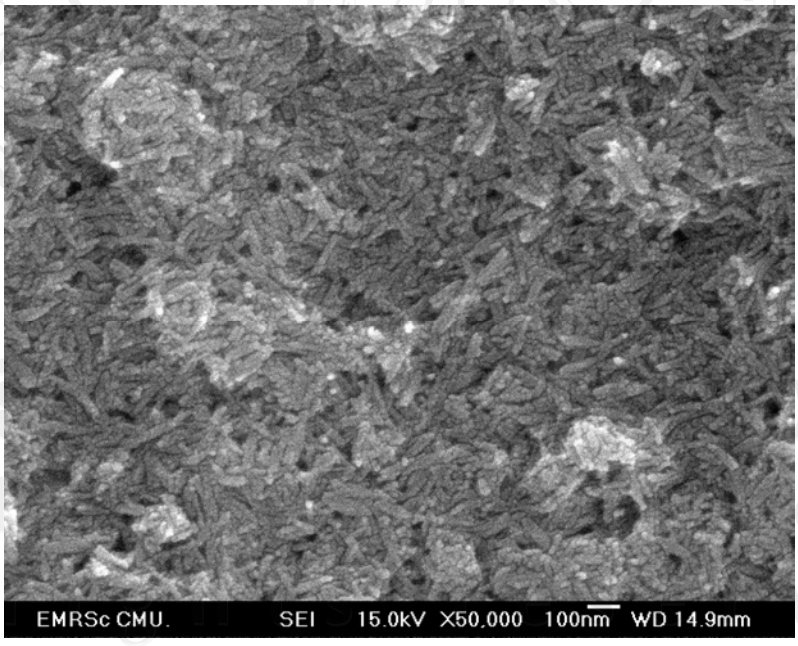

Figure 3.8 SEM image of $LaPO_4$ synthesized in the solution with the pH of 2 by microwave radiation at 180 W for 60 min.

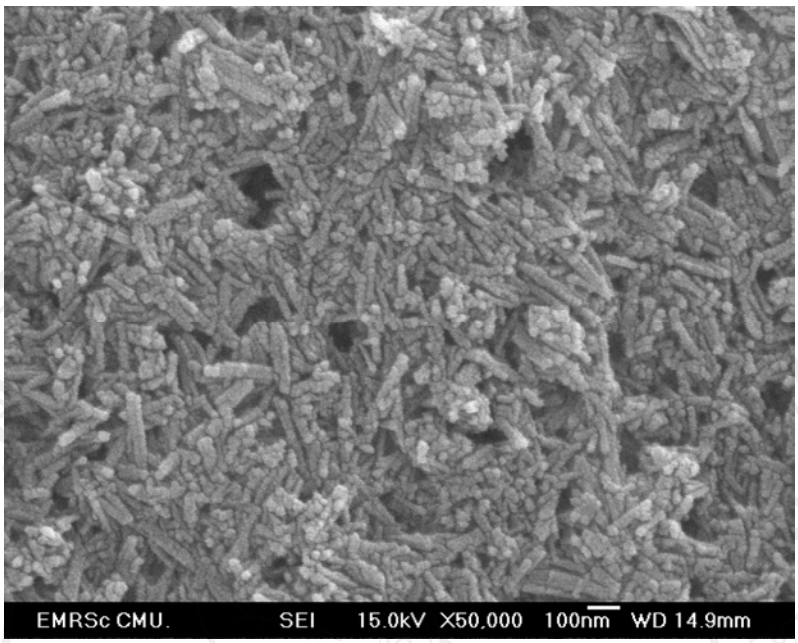

Figure 3.9 SEM image of $LaPO_4$ synthesized in the solution with the pH of 1 by microwave radiation at 180 W for 60 min.

3.1.5 Transmission electron microscope (TEM)

The uniform shape of $LaPO_4$ nanorods was examined by TEM and HRTEM techniques, as shown in Figure 3.10 - 3.13. They indicated the true morphology of $LaPO_4$ at the pH values of 1 and 2, showing that both of these products are nanorods with difference lengths and diameters. The $LaPO_4$ nanorods are 100-200 nm long with 10-12 nm diameters for the pH 2, as shown in Fig. 3.11, and 600-1000 nm long, with 20-40 nm diameters for the pH 1 as shown in Fig. 3.10 - in accordance with those for the same synthesis condition of the SEM analysis. The lattice plane and growth direction of $LaPO_4$ nanorods were analyzed by high-resolution transmission electron microscope (HRTEM), as shown in Fig. 3.12 and 3.13. They show lattice fringes, of

which a number of planes are parallel to the $LaPO_4$ nanorods. They are 4.42 Å apart, corresponding to the (101) plane of hexagonal $LaPO_4$ structure (JCPDS No. 04-0635). This analysis demonstrated that the hexagonal $LaPO_4$ nanorods grew along in [-101] direction.

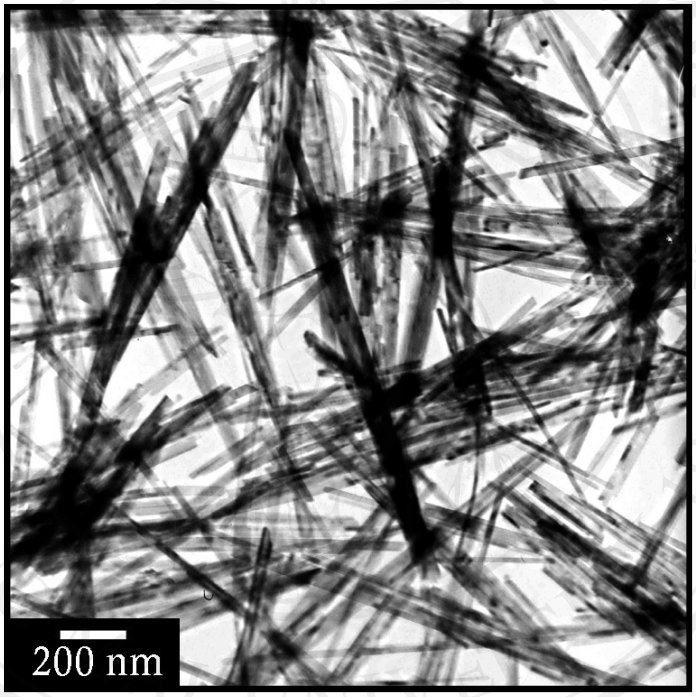

Figure 3.10 TEM image of $LaPO_4$ synthesized in the solution with the pH of 1 by microwave radiation at 180 W for 60 min.

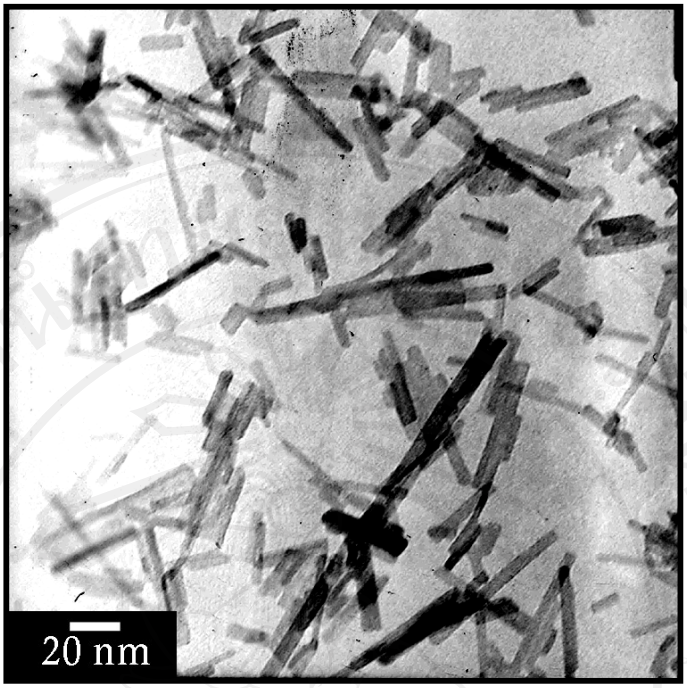

Figure 3.11 TEM image of $LaPO_4$ synthesized in the solution with the pH of 2 by microwave radiation at 180 W for 60 min.

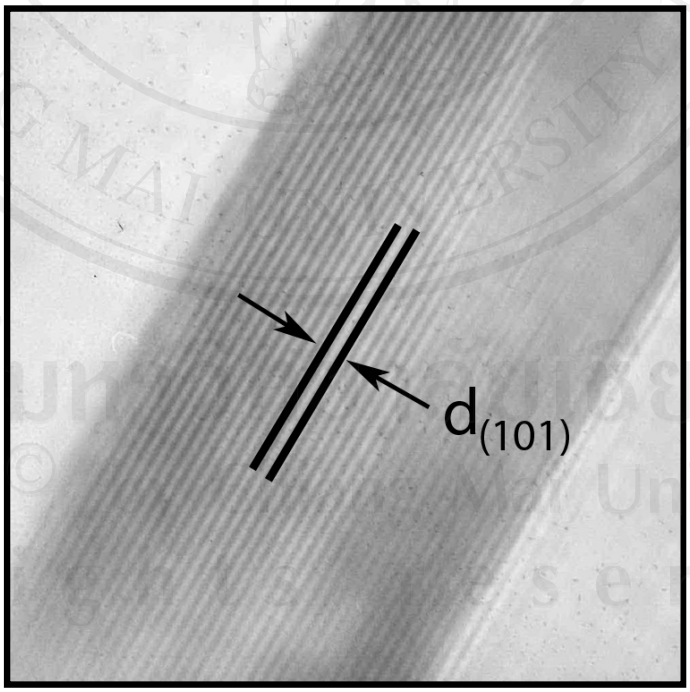

Figure 3.12 HRTEM image of layer of $LaPO_4$ synthesized in the solution with the pH of 1 by microwave radiation at 180 W for 60 min.

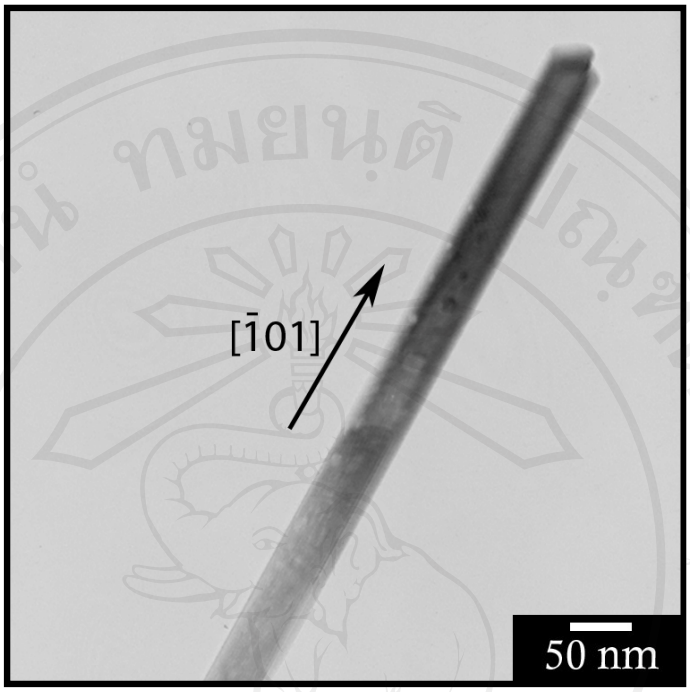

Figure 3.13 HRTEM image of growth direction of $LaPO_4$ synthesized in the solution with the pH of 1 by microwave radiation at 180 W for 60 min.

3.1.6 Possible formation mechanism of Lanthanum Phosphate complex

The effect of pH on different morphologies of nanostructured $LaPO_4$ is illustrated in Figure 3.14

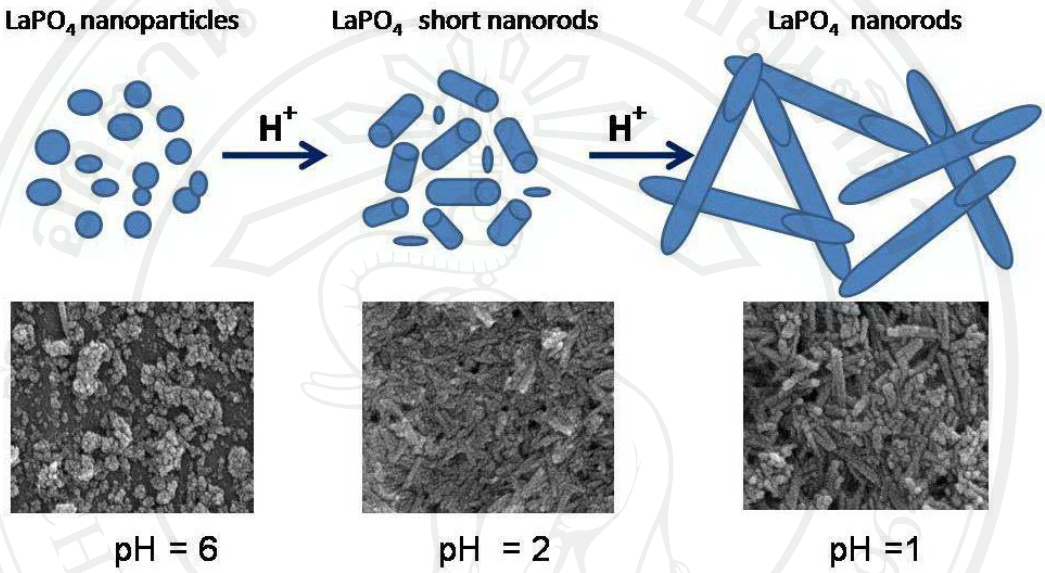

Figure 3.14 Schematic diagram for the formation of $LaPO_4$ products.

A possible formation mechanism of $LaPO_4$ phosphor nanomaterials is simply explained as follows.

$$PO_4^{3-} + nH^+ \rightarrow H_nPO_4^{(3-n)-} \quad (3.3)$$

$$La^{3+} + H_nPO_4^{(3-n)-} \rightarrow LaPO_4\,(\text{white precipitates}) + n\,H^+ \quad (3.4)$$

In this research, $LaCl_3 \cdot 7H_2O$ and $Na_3PO_4 \cdot 12H_2O$ were dissolved in DI water with HNO_3 (conc.) adding. Thus H^+ ions reacted with PO_4^{3-} ions to form $H_nPO_4^{(3-n)-}$,

which subsequently reacted with La^{3+} to produce $LaPO_4$ white precipitates by the microwave radiation at 180 W for 60 min. The products have different morphologies in different pH value solutions. They implied that H^+ concentration induced the system to be at the highest chemical potentials and led the product to grow in 1D $LaPO_4$ nanorods at the pH 1- in accordance with the report of Zhang and Guan [40]. Compared to the facile solution-precipitation process reported by Chai et al. [41], $LaPO_4$ products with different morphologies were synthesized. The effect of the precursor pH on the different morphologies was explained above. In this research, microwave radiation as a heating source has more advantage than the conventional heating process, due to the rapid volumetric heating, resulting in higher reaction rate and selectivity, reduction in reaction time often by orders of magnitude, and increasing yields of the products [42]. It is a candidate for the synthesis of nanomaterials.

The influence of chemical potential on the shape evolution of nanocrystals has been studied by Wang et. al. [43] and Baierlein [44]. In the case of one-dimensional nanostructure growth, it would be advantageous to have a higher chemical potential, which is mainly determined by pH of the solution in our adopted reaction system. Meanwhile ensures a reversible pathway between the fluid phase and the solid phase, which allows atom, ions, or molecules to adopt correct positions in developing crystal lattices.

Control experiments have been carried out to investigate the influence of pH value on the growth of $LaPO_4$ nanorods. A lower pH value implies a higher H^+ ion concentration and higher chemical potential in solution. A higher chemical potential is

preferable for the growth of nanorods, however, higher H^+ ion concentrations may greatly reduce the La^{3+} concentrations, which is restricted by the value of K_{sp} for $LaPO_4$, and thus reduce the rate of ionic motion. Thus, the pH value is the optimal for the preparation of the nanorods [43-44].

3.1.7 Ultraviolet-visible near-infrared spectroscopy (UV-vis NIR)

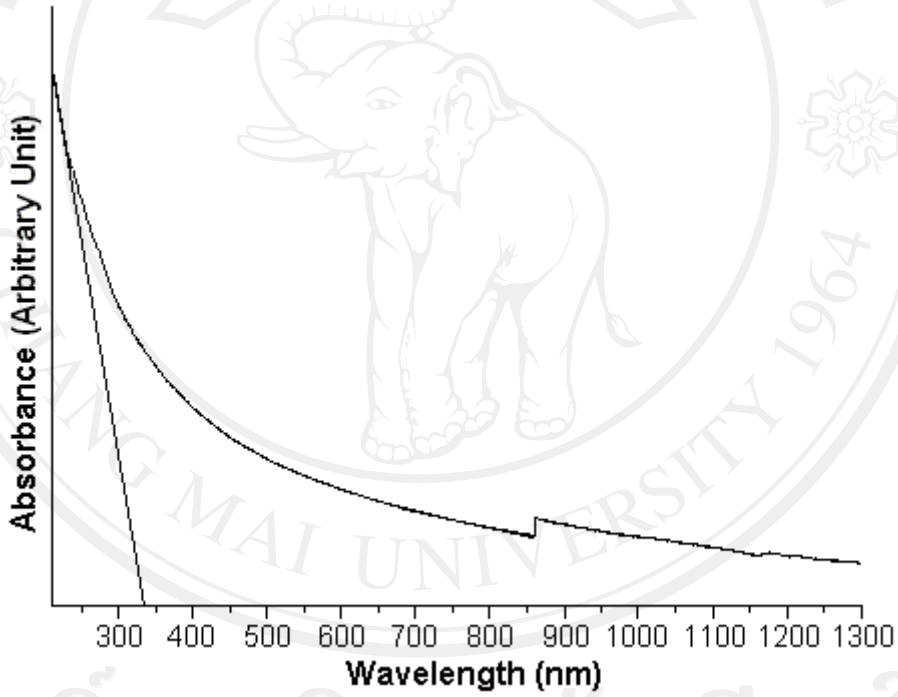

Figure 3.15 UV-vis NIR absorption of $LaPO_4$ nanorods synthesized by microwave radiation at 180 W for 60 min in the solution with the pH of 1.

UV-vis NIR spectroscopic technique was used to characterize the optical properties of $LaPO_4$ nanorods at room temperature. The as-prepared $LaPO_4$ nanorods

were sonicated in absolute ethanol for 15 min, and analyzed the samples over the 200-1300 nm. Figure 3.15 shows the UV-vis NIR of $LaPO_4$ nanorods, which present the absorption in the UV region of 200-1300 nm. The calculated direct band gap (E_g) of $LaPO_4$ nanorods was calculated by the formula below.

$$E_g = 1240 / \lambda_g \qquad (3.5)$$

where λ_g (nm) is the wavelength value corresponding to the intersection point of the vertical and horizontal parts of the spectrum. The band gap of $LaPO_4$ nanorods is 3.64 eV (340 nm) with large red shift relative to the large direct band gap of bulk $LaPO_4$ material of 8.20 eV (151 nm).

3.1.8 Photoluminescent spectroscopy (PL)

Photoluminescent (PL) spectroscopic techniques were used to characterize the optical properties of $LaPO_4$ nanorods at room temperature. The powder of as-prepared $LaPO_4$ nanorods were analyzed over the 300-650 nm range. Figure 3.16 shows the room temperature PL spectrum of $LaPO_4$ nanorods using excitation wavelength of 250 nm. It exhibits a broad luminescence in the major blue and minor green wavelength range. Using Gaussian analysis, the board emission band in 300-650 nm can be disintegrated into four components as two violet, one blue and one green emissions at 370, 410, 468 and 520 nm. The maximum emission is 410 nm of violet range.

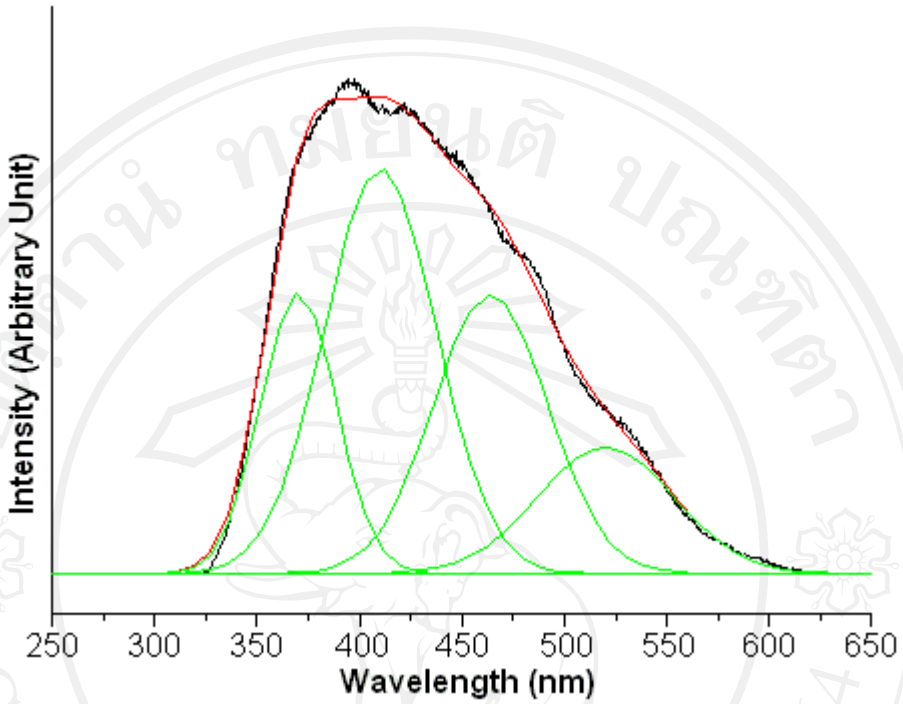

Figure 3.16 PL spectrum of $LaPO_4$ nanorods synthesized by microwave radiation at 180 W for 60 min in the solution with the pH of 1.

3.2 Synthesis of Cerium Phosphate ($CePO_4$) by microwave radiation method

3.2.1 Formation of Cerium Phosphate

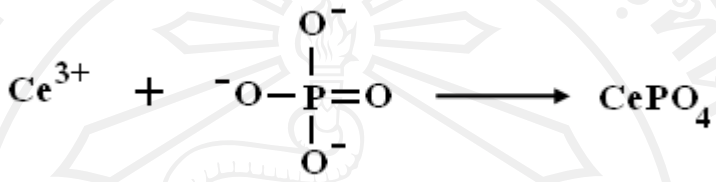

Figure 3.17 Formation of Cerium Phosphate.

In this research, the cerium phosphate ($CePO_4$) complex was prepared by microwave radiation method. Cerium (III) Nitrate hexahydrate ($Ce(NO_3)_3 \cdot 6H_2O$) and tri-sodium phosphate ($Na_3PO_4 \cdot 12H_2O$), the reactants, were dissolved in 80 ml deionized water. Nitric acid (HNO_3) was used to adjust the pH value of the precursor solutions to 1-5. Each of the solutions was continuously heated by a microwave oven at a time at 180 W for 60 min. The final products were analyzed using XRD, FTIR, SEM, TEM, UV-NIR and PL spectroscopy.

Due to the previous research, it showed that the pH value affected the phase purity, crystalline structure and morphology of the complex such as yitrium orthovanadate [22], barium titanate [35], tungsten oxide [36] and so on. In this experiment, the effect of pH value of the precursor solutions on the phase purity, structure, morphology and optical property of the as-synthesized $CePO_4$ was studied.

3.2.2 X-ray diffraction (XRD)

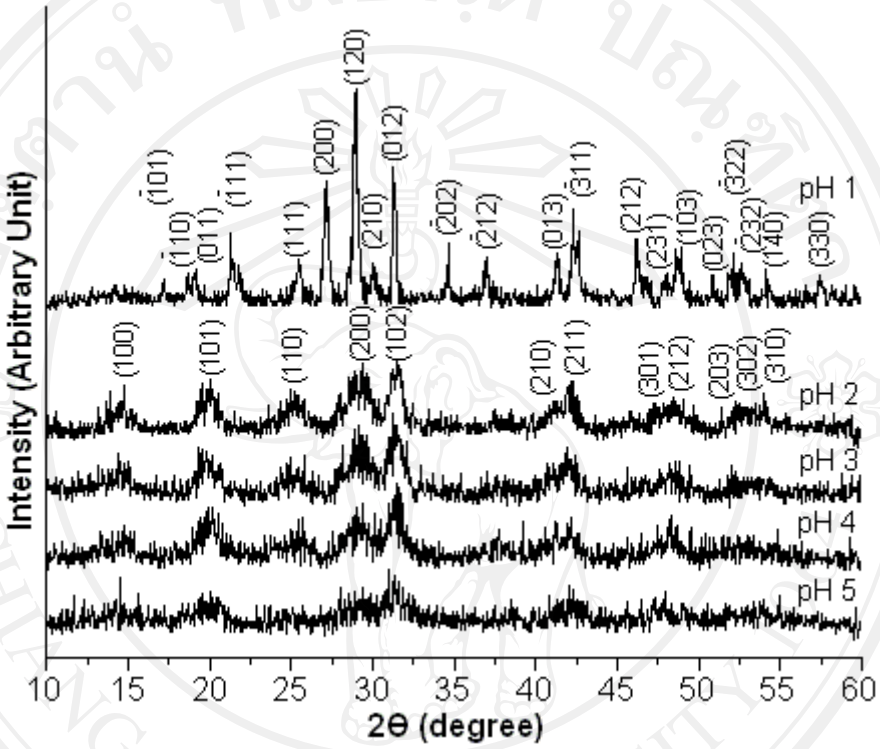

Figure 3.18 XRD patterns of $CePO_4$ synthesized in the solutions with different pH values by microwave radiation at 180 W for 60 min.

Figure 3.18 shows XRD patterns of $CePO_4$ synthesized in the solutions with the pH of 1, 2, 3, 4, and 5 by microwave radiation at 180 W for 60 min. These patterns were specified to correspond with the pure monoclinic $CePO_4$ phase of the JCPDS database No. 77-0429 (a = 6.7700 Å, b = 6.9900 Å, and c = 6.4500 Å, V = 296.67 $Å^3$) for the product synthesized in the solution pH of 1, and hexagonal $CePO_4$

phase of the JCPDS database No. 75-1880 (a = b = 7.0550 Å, and c = 6.4390 Å, V = 277.55 $Å^3$) for the product synthesized in the solution pH of 2, 3, 4, and 5. Their lattice parameters were respectively calculated from plane spacing equations (3.6) and (3.7) for monoclinic and hexagonal structures below.

$$\frac{1}{d^2} = \frac{1}{\sin^2\beta}\left[\frac{h^2}{a^2} + \frac{k^2\sin^2\beta}{b^2} + \frac{l^2}{c^2} - \frac{2hl\cos\beta}{ac}\right] \tag{3.6}$$

$$\frac{1}{d^2} = \frac{4}{3a^2}\left(h^2 + hk + k^2\right) + \frac{1}{c^2}l^2 \tag{3.7}$$

where a, b and c are the lattice parameters, h, k and l the Miller indices, d the plane spacing, β the angle between the a and c axes (103.6 ^{o}). Their lattice parameters are a = 6.7470 Å, b = 7.0026 Å and c = 6.4344 Å for monoclinic $CePO_4$ structure, and a = b = 6.9604 Å and c = 6.4511 Å for hexagonal structure. They are in good accordance with those of the standard. Unit cell volumes (V) were respectively calculated from equations (3.8) and (3.9) for monoclinic and hexagonal $CePO_4$ nanostructures below.

$$\mathrm{V} = abc\sin\beta \tag{3.8}$$

$$\mathrm{V} = a^2 c\sin 60 \tag{3.9}$$

The unit cell volumes are 295.48 $Å^3$ for monoclinic $CePO_4$ and 270.67 $Å^3$ for hexagonal $CePO_4$. It should be noted that the decrease in the cell volume of both monoclinic and hexagonal $CePO_4$ nanostructures indicates that these lattices are more distorted, comparing to the corresponding bulks.

3.2.3 Fourier transform infrared spectroscopy (FT-IR)

FTIR spectra, as shown in Figure 3.19, are the vibrations of PO_4^{3-} tetrahedrons of $CePO_4$ materials at the pH 1, 3 and 5. By using group theory calculation, PO_4^{3-} tetrahedrons has four vibrational modes: The $\upsilon_1(A_1)$, $\upsilon_2(E)$, and $\upsilon_3(F_2)$ are symmetric stretching, symmetric bending and asymmetric stretching modes, and Raman active. The $\upsilon_4(F_2)$ is asymmetric bending mode, and IR active. The symmetry of PO_4^{3-} tetrahedrons in the $CePO_4$ crystals decreases from T_d to C_1, thus the non-IR mode becomes IR active [38]. The vibrations of phosphate (PO_4^{3-}) tetrahedrons in $CePO_4$ crystals were detected over the 400-1400 cm^{-1} range, and appear as three bands at 1057, 617 and 533 cm^{-1}. The first band at 1057 cm^{-1} is assigned as the asymmetric stretching vibration of PO_4^{3-} groups. Other two bands are attributed to the P-O bending vibrations. No vibration of NO_3^- anions from the residual $Ce(NO_3)_3 \cdot 6H_2O$ were detected in these spectra, proving that the as-synthesized $CePO_4$ nanostructures have very high purity. Moreover, two broad bands at 3440 and 1644 cm^{-1} are assigned as the O-H stretching and bending vibrations of H_2O adsorbed on the surface of $CePO_4$ [37-39].

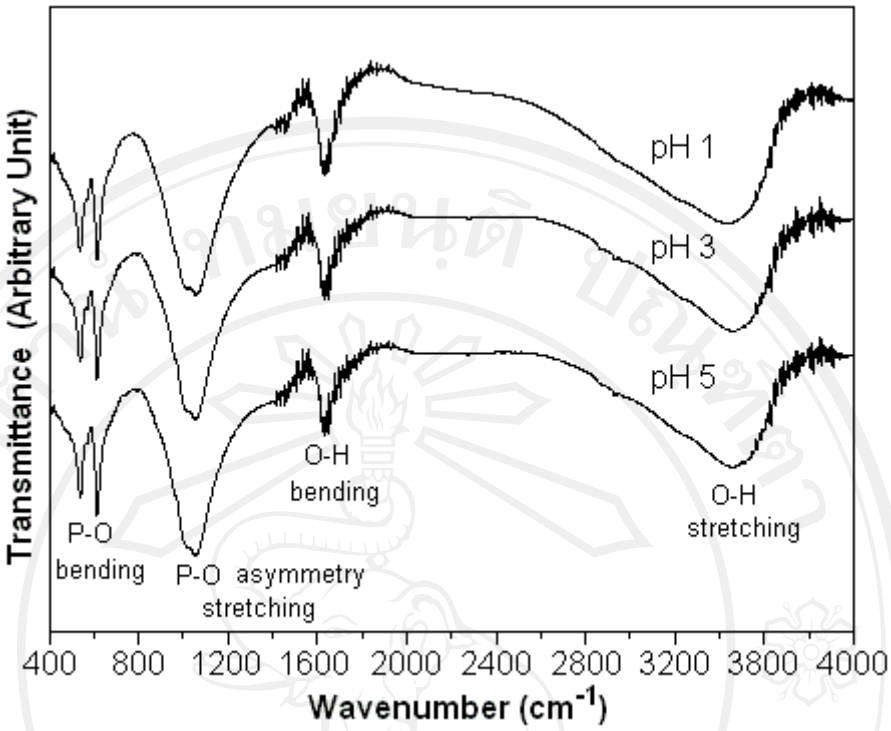

Figure 3.19 FTIR spectra of $CePO_4$ synthesized by microwave radiation method at the pH of 1, 3 and 5.

3.2.4 Scanning electron microscope (SEM)

The influence of pH on the evolution of $CePO_4$ formation was characterized by SEM. The morphologies of the as-synthesized $CePO_4$ images can be classified into two groups, the $CePO_4$ nanoparticles and nanorods in pH ranges of 1-5, as shown in Fig 3.20-3.25. At the pH 3-5, as shown in Fig 3.20-3.22, the products are composed of agglomerated nanoparticles. They became short nanorods at the pH of 1.5-2, as shown in Fig 3.23-3.24. But for the pH of 1, as shown in Fig 3.25, a number of nanorods with 2-3 μm in length and 50 nm in diameter (aspect ratio of 40-60) were synthesized. These results confirmed that pH is a key factor to control the $CePO_4$ morphologies, by

changing from nanoparticles to 1-D nanorods, due to the increase in the H^+ concentration of the solutions as well.

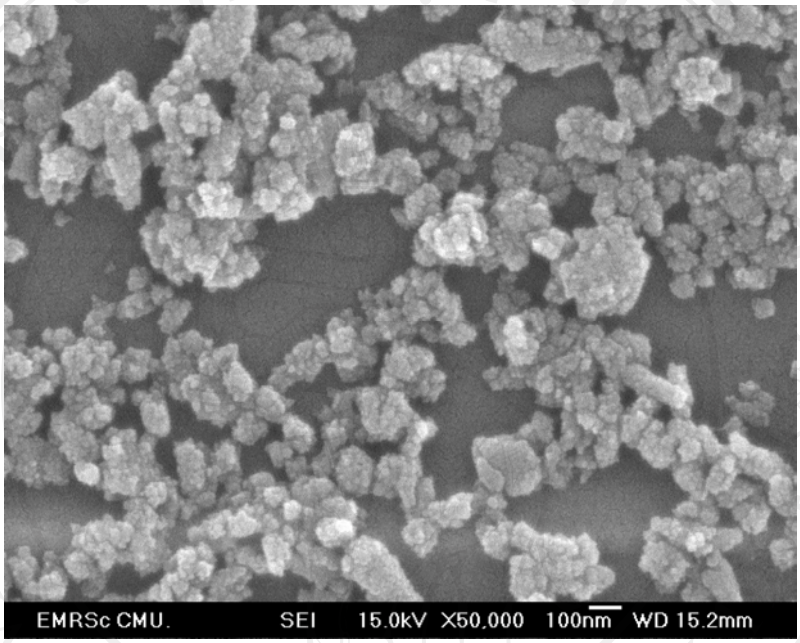

Figure 3.20 SEM image of $CePO_4$ synthesized by microwave radiation method at the pH of 5 by microwave radiation at 180 W for 60 min.

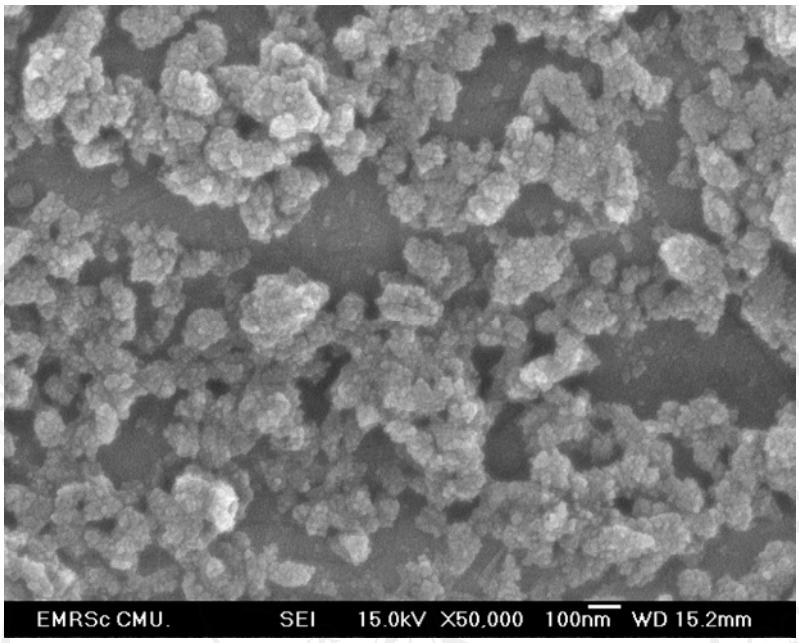

Figure 3.21 SEM image of $CePO_4$ synthesized by microwave radiation method at the pH of 4 by microwave radiation at 180 W for 60 min.

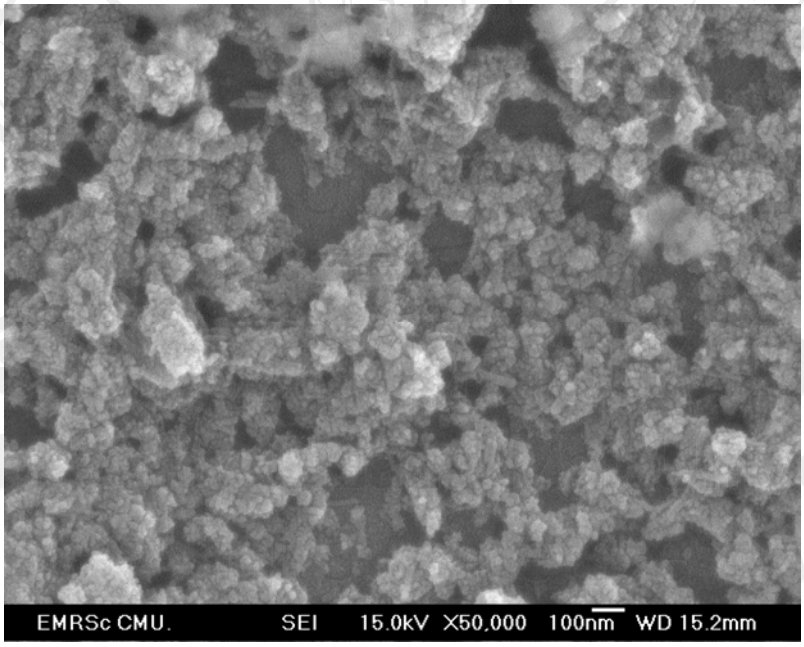

Figure 3.22 SEM image of $CePO_4$ synthesized by microwave radiation method at the pH of 3 by microwave radiation at 180 W for 60 min.

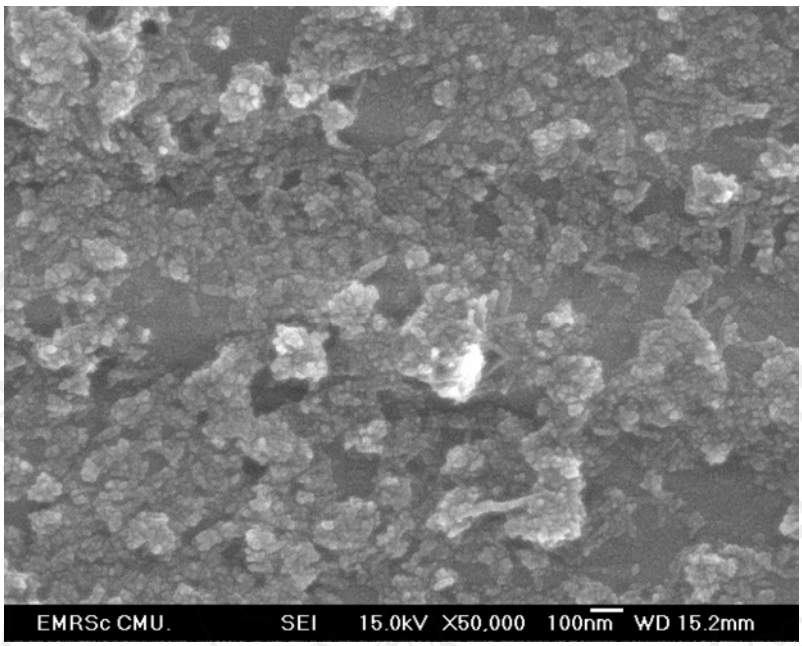

Figure 3.23 SEM image of $CePO_4$ synthesized by microwave radiation method at the pH of 2 by microwave radiation at 180 W for 60 min.

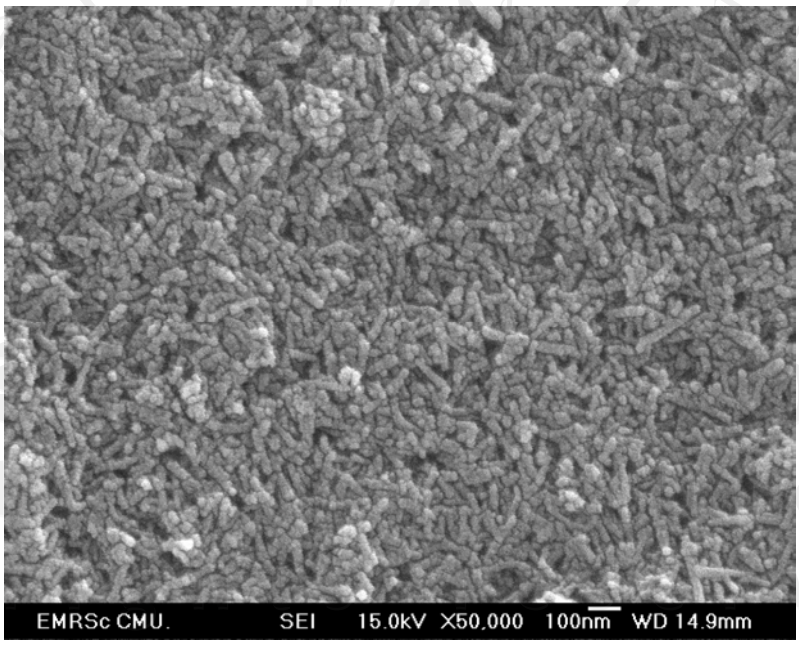

Figure 3.24 SEM image of $CePO_4$ synthesized by microwave radiation method at the pH of 1.5 by microwave radiation at 180 W for 60 min.

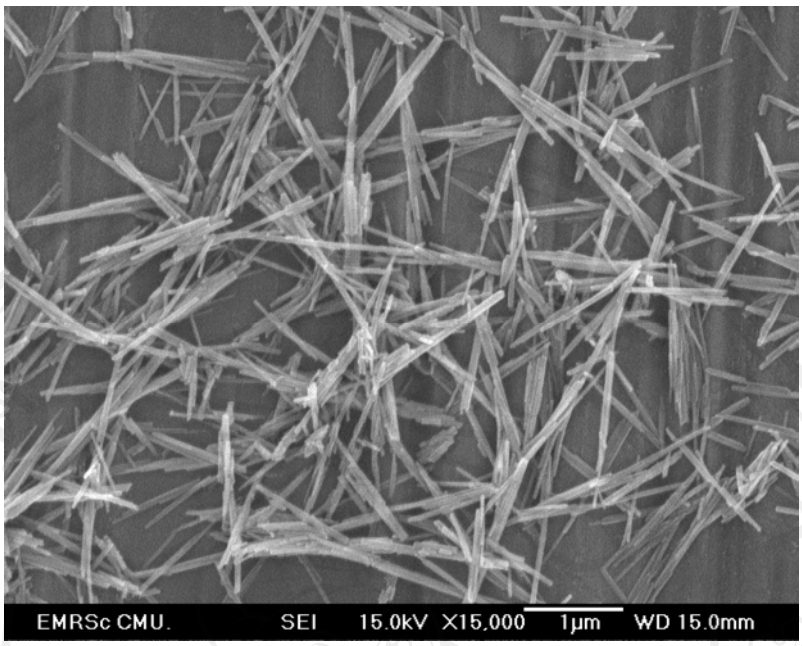

Figure 3.25 SEM image of $CePO_4$ synthesized by microwave radiation method at the pH of 1 by microwave radiation at 180 W for 60 min.

3.2.5 Transmission electron microscope (TEM)

Typical TEM images of the $CePO_4$ products for the pH of 1, 1.5 and 2 are shown in Figure 3.26-3.28. All $CePO_4$ products were nanorods with the diameter and length of several nanometers. Their diameter and length are ~ 10 nm and ~120 nm for the pH 1, ~7.5 nm and ~80 nm for the pH 1.5, and ~5 nm and ~50 nm for the pH 2. These results indicated that lower pH value of precursors solution led the product grew in one dimension.

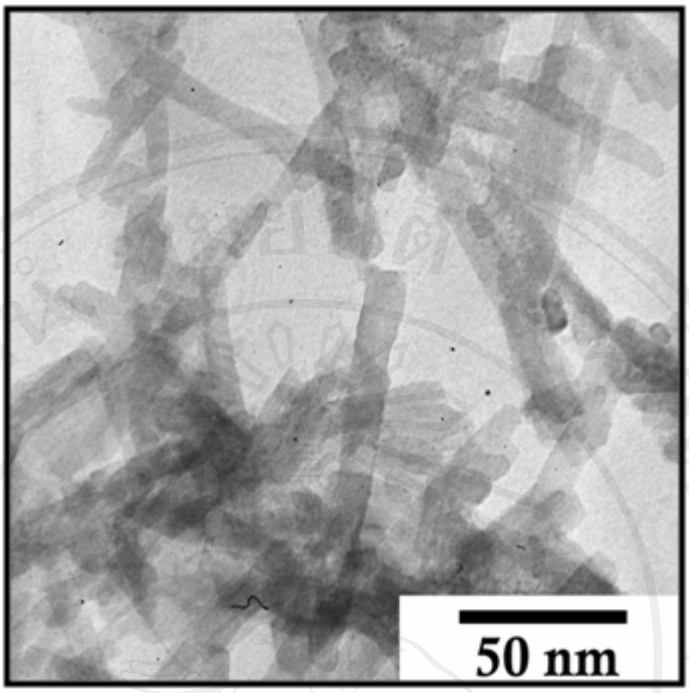

Figure 3.26 TEM image of $LaPO_4$ synthesized in the solution with the pH of 1 by microwave radiation at 180 W for 60 min.

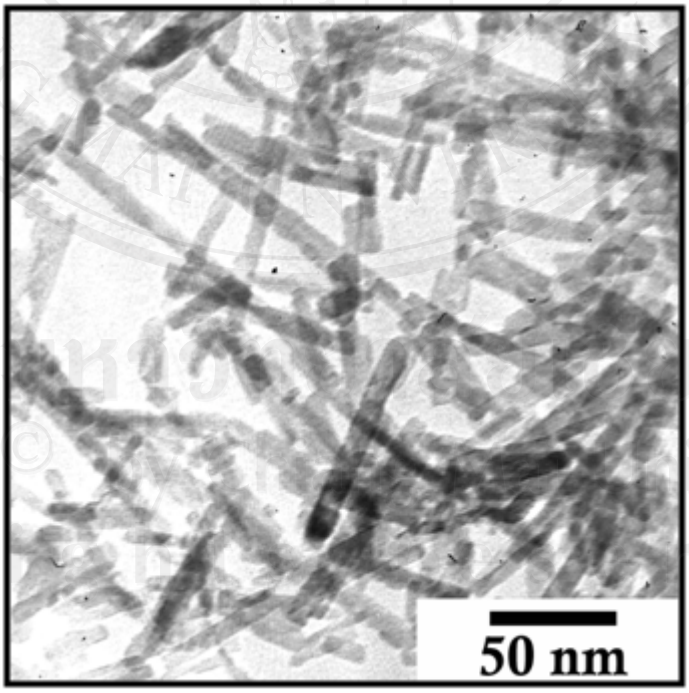

Figure 3.27 TEM image of $LaPO_4$ synthesized in the solution with the pH of 1.5 by microwave radiation at 180 W for 60 min.

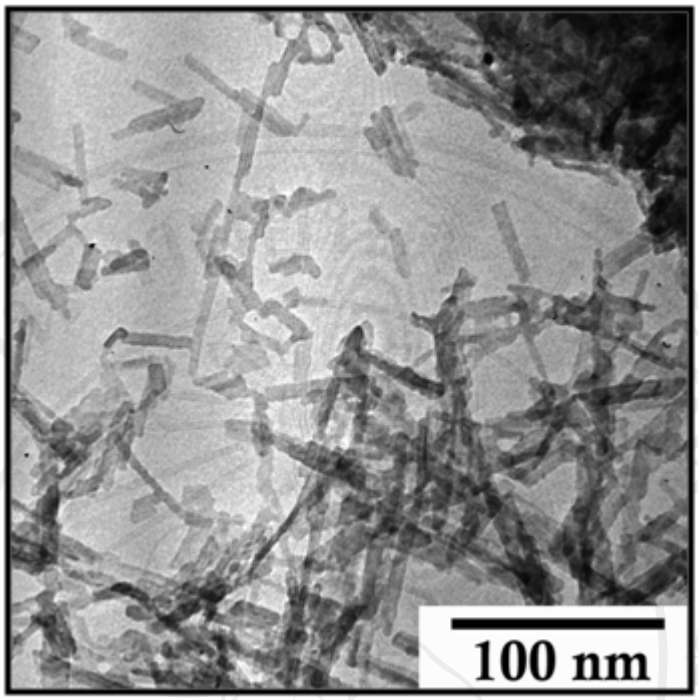

Figure 3.28 TEM image of $LaPO_4$ synthesized in the solution with the pH of 2 by microwave radiation at 180 W for 60 min.

3.2.6 Possible formation mechanism of Cerium Phosphate complex

The effect of pH on different morphologies of $CePO_4$ nanostructures can be illustrated in Figure 3.29.

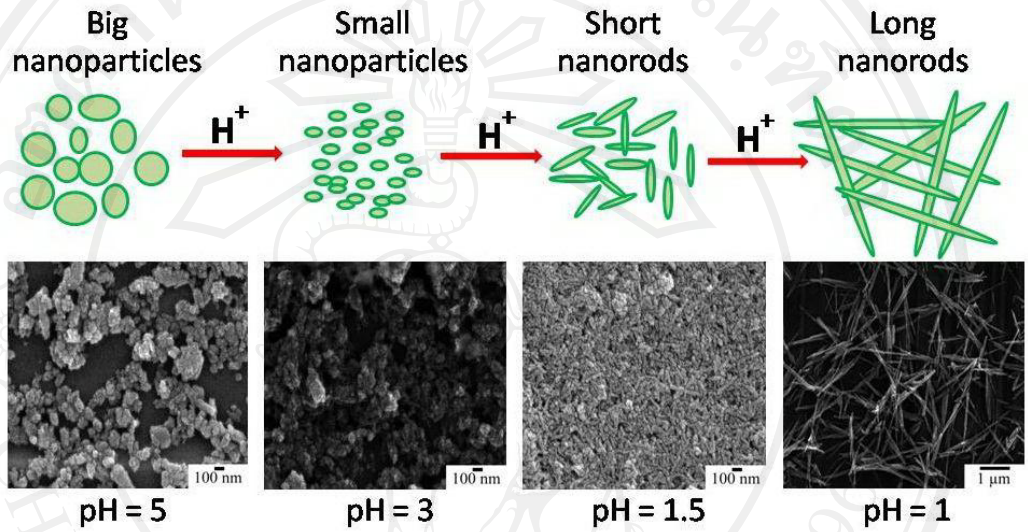

Figure 3.29 Schematic diagram for the formation of $CePO_4$ products.

On the basis of the experimental results, a possible formation mechanism of 1D $CePO_4$ phosphor nanomaterials can be explained as in the equations below.

$$PO_4^{3-} + nH^+ \rightarrow H_nPO_4^{(3-n)-} \quad (3.10)$$

$$Ce^{3+} + H_nPO_4^{(3-n)} \rightarrow CePO_4 \text{ (green precipitates)} + nH^+ \quad (3.11)$$

Generally, shape of the product is controlled by the kinetics and thermodynamics. In this case, the formation of $CePO_4$ nanorods can be explained in term of the thermodynamics, relating to the chemical potential. The influence of

chemical potential on the shape evolution of nanocrystals was discussed by Wang et al [43], Baierlein [44] and Peng et al [45]. By adding HNO_3 (conc.) to the precursors, until the pH was 1. At this condition, Ce^{3+} and $H_nPO_4^{(3-n)-}$ concentrations became higher, and the solution was higher chemical potentials. Thus, the 1D $CePO_4$ nanorods were finally synthesized under the microwave radiation.

In this research, we were investigated the influence of pH value on the growth of $CePO_4$ nanorods. A low pH value implies a higher H^+ concentration and higher chemical potential in solution. A higher chemical potential is preferable for the growth of nanorods, however, higher H^+ concentrations may greatly reduce the Ce^{3+} concentrations, which is restricted by the value of K_{sp} for $CePO_4$, and thus reduce the rate of ionic motion. The pH value is optimal for the preparation of nanorods. Meanwhile ensures a reversible pathway between the fluid and the solid phases, which allows atom, ions, or molecules to adopt correct positions in developing crystal lattices [42-45].

3.2.7 Ultraviolet-visible near-infrared spectroscopy (UV-vis NIR)

Figure 3.30 shows UV-visible spectrum of the monoclinic $CePO_4$ nanorods for the solution pH of 1 in the range of 200-650 nm wavelength. In general, the optical absorption of $CePO_4$ material has two electron transition modes in the f-f orbital appearing in the IR region (λ_{max}~440 nm), and the f-d transition in the ultraviolet region (λ~190-300 nm) [9]. Two strong absorption peaks at 216 and 277 nm coupled with two small shoulder peaks at 238 and 260 nm in ultraviolet region of the as-synthesized $CePO_4$ nanorods were detected, due to the 4f-5d electron transitions of Ce^{3+} atoms in $CePO_4$ lattice. The energy level for Ce^{3+} ion (insert of Fig. 3.30(a)) shows three electron transitions as $^2F_{5/2} \rightarrow {}^2F_{7/2}$, $^2F_{5/2} \rightarrow {}^2D_{3/2}$, and $^2F_{5/2} \rightarrow {}^2D_{5/2}$. The lowest energy transition ($^2F_{5/2} \rightarrow {}^2F_{7/2}$) is a Laporte forbidden n to n transition corresponding to the f^n to f^n transition. The other two electron transitions, $^2F_{5/2} \rightarrow {}^2D_{3/2}$ and $^2F_{5/2} \rightarrow {}^2D_{5/2}$ are Laporte allowed (n-1)f to nf-d transitions. For two major absorption peaks of $CePO_4$ nanorods at 216 and 277 nm are assigned to be $^2F_{5/2} \rightarrow {}^2D_{3/2}$ and $^2F_{5/2} \rightarrow {}^2D_{5/2}$. Moreover, the shoulder peaks at 238 and 260 nm overlapped the excited state was strongly spit by the crystal field effect. The electronic transition of $^2F_{5/2} \rightarrow {}^2F_{7/2}$ was not detected [12]. The direct band gap of $CePO_4$ nanorods (Fig. 3.30 b) was determined from the plot of $(\alpha h\nu)^2$ vs hv, where α is the absorbance, h the Planck constant, and v the frequency. The direct band gap (E_g) of $CePO_4$ nanorods is 4.1 eV – in accordance with the previous reports [12,23,46].

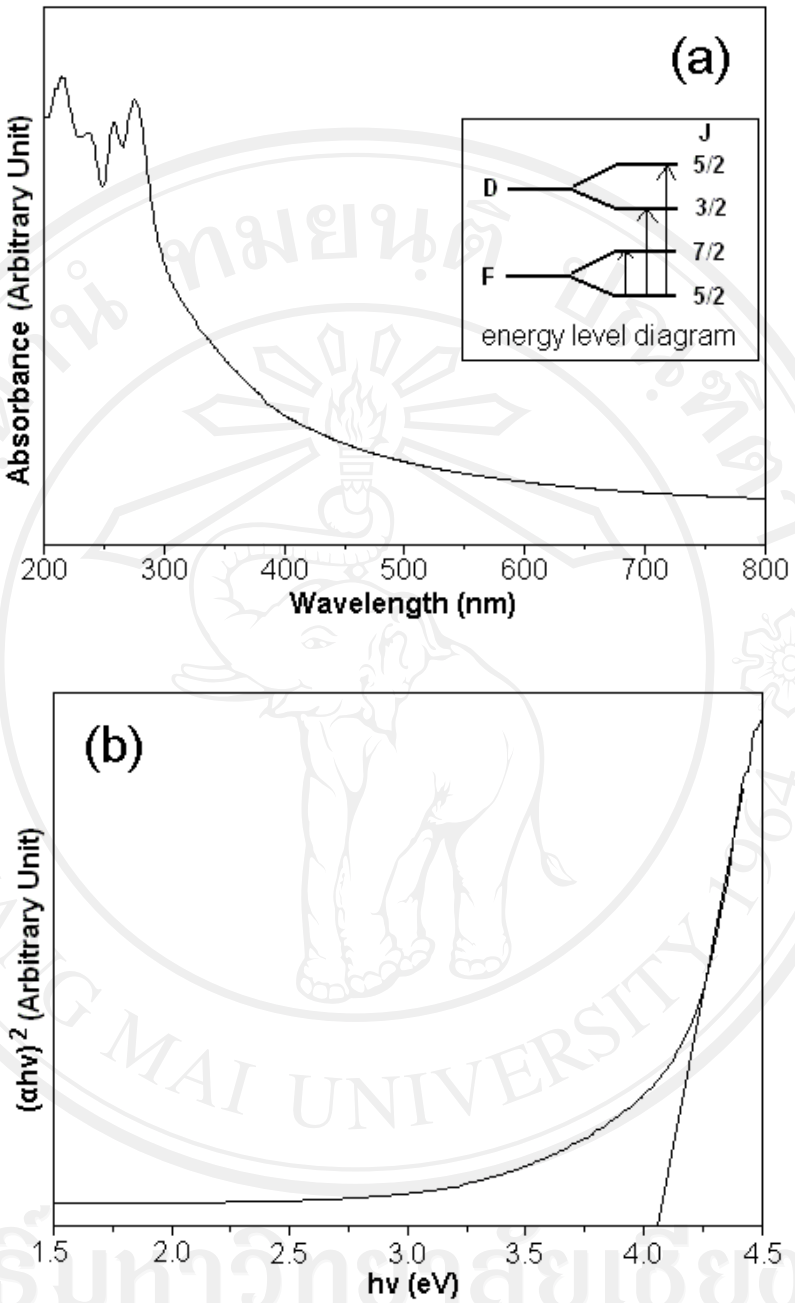

Figure 3.30 (a) UV-vis absorption, and (b) $(\alpha hv)^2$ vs hv curve of $CePO_4$ nanorods synthesized in the solution pH of 1, using microwave radiation at 180 W for 60 min.

3.2.8 Photoluminescent spectroscopy (PL)

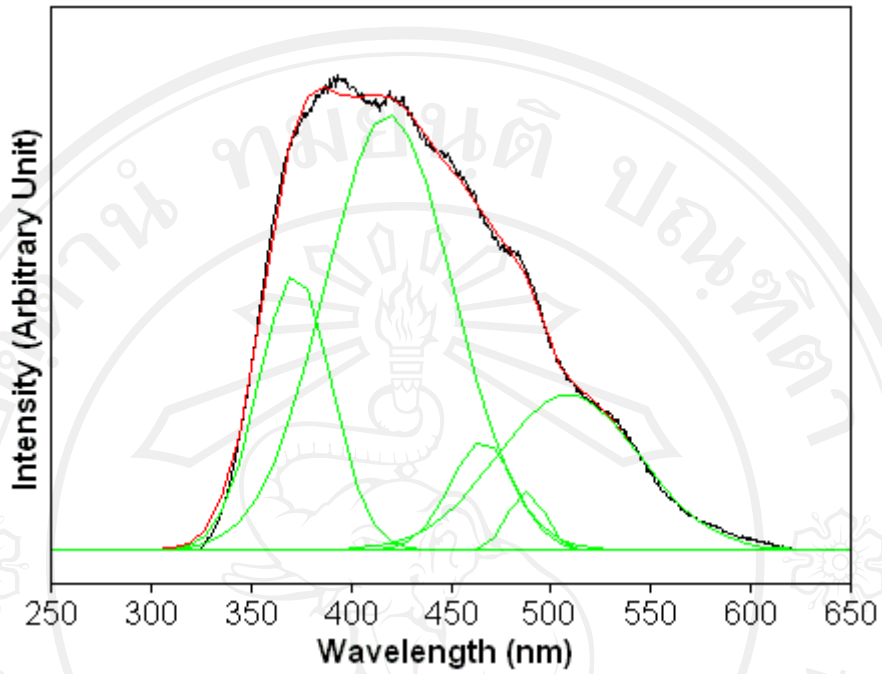

Figure 3.31 PL spectrum of $CePO_4$ nanorods synthesized in the solution pH of 1, using microwave radiation at 180 W for 60 min.

The room temperature photoluminescence of $CePO_4$ nanorods was investigated using an excitation wavelength of 250 nm as shown in Fig. 3.31. It should be noted that the PL curve exhibits a broad luminescent band in the major blue, and minor violet and green wavelength range. Similar results were detected in the collective emission spectra of rare earth phosphates. By using Gaussian analysis, the broad emission band in 300-650 nm can be separated into five components at 372, 419, 466, 488 and 509 nm. Each represents the different type of electronic transitions, linked with the structural arrangement or surface defects.